J Solid State Electrochem (2012) 16:3147–3157
DOI 10.1007/s10008-012-1755-y

ORIGINAL PAPER

Microwave-assisted polyol synthesis of carbon-supported platinum-based bimetallic catalysts for ethanol oxidation

S. Stevanović · D. Tripković · J. Rogan · K. Popović · J. Lović · A. Tripković · V. M. Jovanović

Received: 10 October 2011 / Revised: 18 April 2012 / Accepted: 18 April 2012 / Published online: 5 May 2012
© Springer-Verlag 2012

Abstract High surface area carbon-supported Pt, PtRh, and PtSn catalysts were synthesized by microwave-assisted polyol procedure and tested for ethanol oxidation in perchloric acid. The catalysts were characterized by thermogravimetric analysis (TGA), X-ray diffraction (XRD), scanning tunnelling microscopy (STM), TEM, and EDX techniques. STM analysis of unsupported catalysts shows that small particles (~2 nm) with a narrow size distribution are obtained. TEM and XRD examinations of supported catalysts revealed an increase in particle size upon deposition on carbon support (diameter~3 nm). The diffraction peaks of the bimetallic catalysts in X-ray diffraction patterns are slightly shifted to lower (PtSn/C) or higher (PtRh/C) 2θ values with respect to the corresponding peaks at Pt/C catalyst as a consequence of alloy formation. Oxidation of ethanol is significantly improved at PtSn/C with the onset potential shifted for~150 mV to more negative values and the increase of activity for approximately three times in comparison to Pt/C catalyst. This is the lowest onset potential found for ethanol oxidation at PtSn catalysts with a similar composition. Chronoamperometric measurements confirmed that PtSn/C is notably less poisoned than Pt/C catalyst. PtRh/C catalyst exhibited mild enhancement of overall electrochemical reaction in comparison to Pt/C.

S. Stevanović · D. Tripković · K. Popović · J. Lović · A. Tripković · V. M. Jovanović (✉)
ICTM, Department of Electrochemistry, University of Belgrade, Njegoševa 12,
Belgrade, Serbia
e-mail: vlad@tmf.bg.ac.rs

J. Rogan
Faculty of Technology and Metallurgy, University of Belgrade, Karnegijeva 4,
Belgrade, Serbia

Keywords PtSn/C · PtRh/C · Ethanol oxidation · Polyol synthesis · Microwave irradiation

Introduction

Limited sources of fossil fuels as well as the request for reduction of environmental pollution led to the development of alternative energy sources, such as fuel cells. Although the best performance, so far, has been achieved using hydrogen as fuel, its storage, handling, and distribution appear to be important barriers for direct and widespread application. Direct use of liquid fuels, such as methanol, ethanol, and formic acid, has been studied as a convenient alternative. Ethanol is receiving increasing attention due to its low toxicity and large quantity production from the fermentation of biomass as a renewable biofuel [1]. However, to oxidize ethanol efficiently, it is necessary to develop a catalyst capable for converting it completely to CO_2. Pt is an excellent catalyst for dehydrogenation of small organic molecules but, on the other hand, has several significant drawbacks: high cost, extreme susceptibility to poisoning by CO, and, in the case of ethanol, the main products of its oxidation are acetaldehyde and acetic acid, while CO_2 is produced at high potentials [2]. Efforts to improve catalyst performance and minimize quantity of Pt in the catalyst have been centered on the addition of metals such as Ru, Rh, W, Pd, Sn, etc. [1–10].

PtSn is one of the extensively studied and among the most active bimetallic catalysts for ethanol oxidation. The activity of PtSn is attributed to a bifunctional mechanism in which alcohol is adsorbed and dehydrogenated at Pt, while added metal supplies OH at significantly lower potentials compared to Pt, providing oxidation of adsorbed reaction intermediates (CO-like species strongly adsorbed on adjacent Pt active sites) leading to carbon dioxide, in the situation that the C–C bond

was broken and the formation of acetaldehyde and acetic acid was suppressed [11, 12]. Besides, the electronic interaction between Pt and alloyed metal results in a weaker bond of adsorbed species on Pt and contributes to enhanced activity of these catalysts [12–16]. While there is no doubt in the beneficial role of the bifunctional mechanism in increased activity of PtSn catalyst for ethanol oxidation, this view on alloying effect is rather controversial. According to some authors, higher alloying degree leads to a larger increase in activity of the PtSn catalyst [14, 15], whereas for others, unchanged lattice parameter of Pt in nonalloyed Pt-SnO_x catalysts enables remarkable promotion of ethanol oxidation [17–19]. However, although affecting the overall electrochemical activity in ethanol oxidation, addition of Sn does not enhance the yield of CO_2, i.e., C–C bond braking as revealed by differential mass spectrometry (DEMS) and in situ infrared spectroscopy (FTIR) [2, 7, 13].

On the other hand, addition of Rh to Pt leads to increased ratio of CO_2/acetaldehyde and CO_2/acetic acid as evidenced by DEMS and FTIR techniques, which is ascribed to improved activation of C–C bond dissociation [9, 20]. At the same time, the overall electrochemical reaction is not enhanced by the PtRh/C catalyst possibly because of a stronger CO–Rh bond and/or slower dehydrogenation of ethanol at Rh in comparison to Pt [21].

In general, electrocatalytic performance of the Pt-based catalysts considerably depends not only on the nature of the added metal but also on a variety of conditions of the synthesis procedures which determine surface composition and morphology of synthesized materials. In the last decade, polyol method has been often used for the preparation of Pt or Pt-based nanoclusters with small particle size and narrow size distribution [22]. In this procedure, ethylene glycol (EG) and hydroxide are used as stabilizers. EG acting as both reaction and dispersion media can efficiently adsorb and stabilize the surface of the particles [23] and favor formation of metal particles with good dispersivity [24, 25]. Since EG has high permanent dipole, it is very susceptible to microwave irradiation, which can take up the energy from the microwave field and get the polar reaction solution heated up to high temperature instantaneously [26]. The fast and uniform microwave heating reduces the temperature and concentration gradients, thus accelerating the reduction of the metal ions and enabling homogeneous nucleation and shorter crystallization time leading to formation of small uniform metal particles [27–30].

In this work, as-prepared carbon-supported nanoparticles, Pt, PtRh, and PtSn catalysts, synthesized by microwave-assisted polyol method, were characterized for ethanol electrooxidation reaction. Although microwave-assisted synthesis of Pt/C and PtSn/C catalyst has been described in literature [28, 31], to our knowledge, only recently have such catalysts been studied for ethanol oxidation [32]. This reaction has not been examined by PtRh/C catalyst prepared by microwave irradiation so far.

Experimental

Preparation of the catalysts

Stabile Pt, PtRh, and PtSn nanoparticles were prepared by polyol method. Briefly, equal volumes of 0.05 M water solutions of required metal precursor salts (H_2PtCl_6 alone or either with $SnCl_2$ or $RhCl_3$) were mixed with EG, and NaOH was added dropwise. The solutions mixture was constantly stirred. In this way, EG/water ratio was 20/1, NaOH/metal ratio 8/1, and pH of the solutions adjusted to over 12. The prepared solutions were heated in a microwave oven at 700 W for 60 s (Pt) or 90 s (bimetallic). After microwave heating, colloidal solutions were uniformly mixed with water suspension of high-area carbon (Vulcan XC-72) and 2 M H_2SO_4 solution and stirred for 3 h. The resulting suspension was filtered, and the residue was rinsed with high purity water. The solid product was dried at 160 °C for 3 h in N_2 atmosphere. In all cases, the amount of metal and carbon was adjusted to the loading of 20 mass% of the catalyst.

Characterization of the catalysts

The thermogravimetric (TGA) and differential thermal (DTA) analyses were performed simultaneously (30–800 °C range) on a SDT Q600 TGA/DSC instrument (TA Instruments). The heating rates were 20 °C min^{-1}, and the sample mass was less than 10 mg. The furnace atmosphere consisted of air at a flow rate of 100 cm^3 min^{-1}.

Unsupported Pt, PtRh, and PtSn nanoparticles were characterized by scanning tunnelling microscopy (STM). Samples were prepared by applying a few drops of a diluted colloidal solution of a catalyst on a hot HOPG plate. STM characterizations were performed using a NanoScope III A (Veeco, USA) microscope. The images were obtained in the height mode using a Pt-Ir tip (set-point current, i_t, from 1 to 2 nA, bias voltage, V_b=−300 mV). The mean particle size and size distribution were acquired from a few randomly chosen areas in the STM images containing about 100 particles.

The X-ray diffraction (XRD) patterns of the powder catalysts were recorded with an Ital Structure APD2000 X-ray diffractometer in a Bragg–Brentano geometry using CuKα radiation (λ=1.5418 Å) and step-scan mode (range: 15−85 ° 2θ, step-time: 2.50 s, step-width: 0.02 °). The program PowderCell [33] was used for phase analysis and calculation of unit cell parameters.

Structural examination of the catalysts was performed by EDX technique coupled with scanning electron microscopy using JEOL JSM-6610 (USA) instrument with X-Max

(silicon drift) detector and super atmospheric thin window (SATW) applying 20 kV. The measurements were performed at ten different regions of each sample.

TEM analysis of the supported catalysts was carried out using a Philips CM12 TEM microscope (The Netherlands) operated at 100 kV. The samples were prepared by ultrasonically dispersing the catalysts powders in ethanol and applying a drop of the suspension onto the carbon-coated copper grid. The size distribution of the catalysts particles were created based on 450 particles from a few different areas of the sample for each catalyst.

Electrochemical measurements

All of the electrochemical experiments were performed at room temperature in a three-electrode compartment electrochemical cell with a Pt wire as the counter electrode and a bridged saturated calomel electrode (SCE) as reference. The working electrode was a thin layer of Nafion-impregnated Pt/C, PtRh/C, or PtSn/C catalysts applied on a polished glassy carbon disk electrode with 20 $\mu g/cm^2$ loading of the catalyst. The thin layer was obtained from a suspension of 2 mg of the respective catalyst in a mixture of 1 ml water and 50 μl of 5 % aqueous Nafion solution, prepared in an ultrasonic bath, placed onto the substrate and dried at room temperature.

The electrocatalytic activity of as-prepared Pt/C, PtRh/C, and PtSn/C was studied in 0.1 M $HClO_4$+0.5 M C_2H_5OH solution. Ethanol was added to the supporting electrolyte solution while holding the electrode potential at −0.2 V. The potential was then cycled up to 0.3 V, i.e., the potential range of technical interest (E<0.4 V), as well as up to 0.8 V at a sweep rate of 20 mV/s. Current–time transient curves were recorded after immersion of the freshly prepared electrode in the solution at −0.2 V for 2 s followed by stepping the potential to 0.2 V and holding the electrode at that potential for 30 min.

The real surface area of all as-prepared catalysts was calculated from CO stripping voltammetry. For the CO stripping measurements, pure CO was bubbled through the electrolyte for 30 min while keeping the electrode potential at −0.2 V versus SCE. After purging the electrolyte by N_2 for 30 min to eliminate the dissolved CO, the adsorbed CO was oxidized in an anodic scan (50 mV/s). Two potential cycles were recorded to verify the completeness of the CO oxidation. The real surface area was estimated by the calculation of the charge from CO_{ads} stripping voltammograms (assuming 420 $\mu C/cm^2$ for the CO monolayer). Assuming that the active surface area determined in this way is equal to the area for ethanol oxidation [2, 13], the specific catalysts activities are normalized with respect to values obtained.

All the solutions were prepared from p.a. reagents with high purity water. The electrolytes were purged with purified nitrogen prior to each experiment. Autolab potentiostat/galvanostat (Eco Chemie, The Netherlands) was used in electrochemical experiments.

Results and discussion

Characterization of the catalysts

STM was used in order to characterize the particle size and surface morphology of as-prepared Pt, PtRh, and PtSn catalysts synthesized from colloidal solutions by microwave irradiation before their deposition onto the carbon support. As observed from the top view of STM images (Fig. 1), all catalysts have rather uniform particles of a small diameter. Most particles are in spherical shape. The particle size distribution, evaluated through cross-section analysis (Fig. 1) based on statistics of over 100 particles for each catalyst, confirmed particle size of below 2 nm for both Pt and PtSn catalysts and somewhat over 2 nm for PtRh as well as narrow size distribution for all catalysts. The small particle sizes and homogeneous size distributions of all catalysts should be attributed to the advantages of microwave-assisted modified polyol process in EG solution. The dielectric constant (41.4 at 298 K) and the dielectric loss of EG are high, and hence, rapid heating occurs easily under microwave irradiation [34]. In polyol process, EG acts as a reaction agent to reduce the metal ions to metal powders [35]. In this procedure, hydroxide is used as stabilizer, and thus, pH value of the solution as well as hydroxide/metal molar ratio is very important for obtaining stable metal particles [22]. EG with its high viscosity also helps in preventing agglomeration of the nanoparticles, and for this reason, the water content in reaction solution effects this process as well as the reaction temperature influencing the particle size and size distribution [25]. Thus, fast and uniform microwave heating accelerated the reduction of the metal ions, and together with chosen EG/water and NaOH/metal ratios greatly facilitated small and uniform particle formation.

XRD patterns of the carbon-supported Pt and Pt-based catalysts (Fig. 2) show main characteristic peaks of face-centered cubic (fcc) Pt crystalline structure and the diffraction peak at around 25 ° related to graphitelike structure of Vulcan support. The slight shift of the diffraction peaks of PtSn/C and PtRh/C catalysts to lower and higher 2θ values, respectively, with respect to the corresponding values for Pt/C can be observed. The lattice parameters of all the catalysts are listed in Table 1, and as can be seen, the lattice parameter for PtSn/C is enlarged, while PtRh/C has a smaller one regarding to Pt/C. This indicates that the addition of Sn or Rh to Pt has a different effect on the Pt crystal structure that can be explained by their different atomic sizes. Since Sn and Rh has bigger and smaller atomic radii, respectively, than Pt, their addition would induce extension or contraction of Pt lattice, respectively. The slight

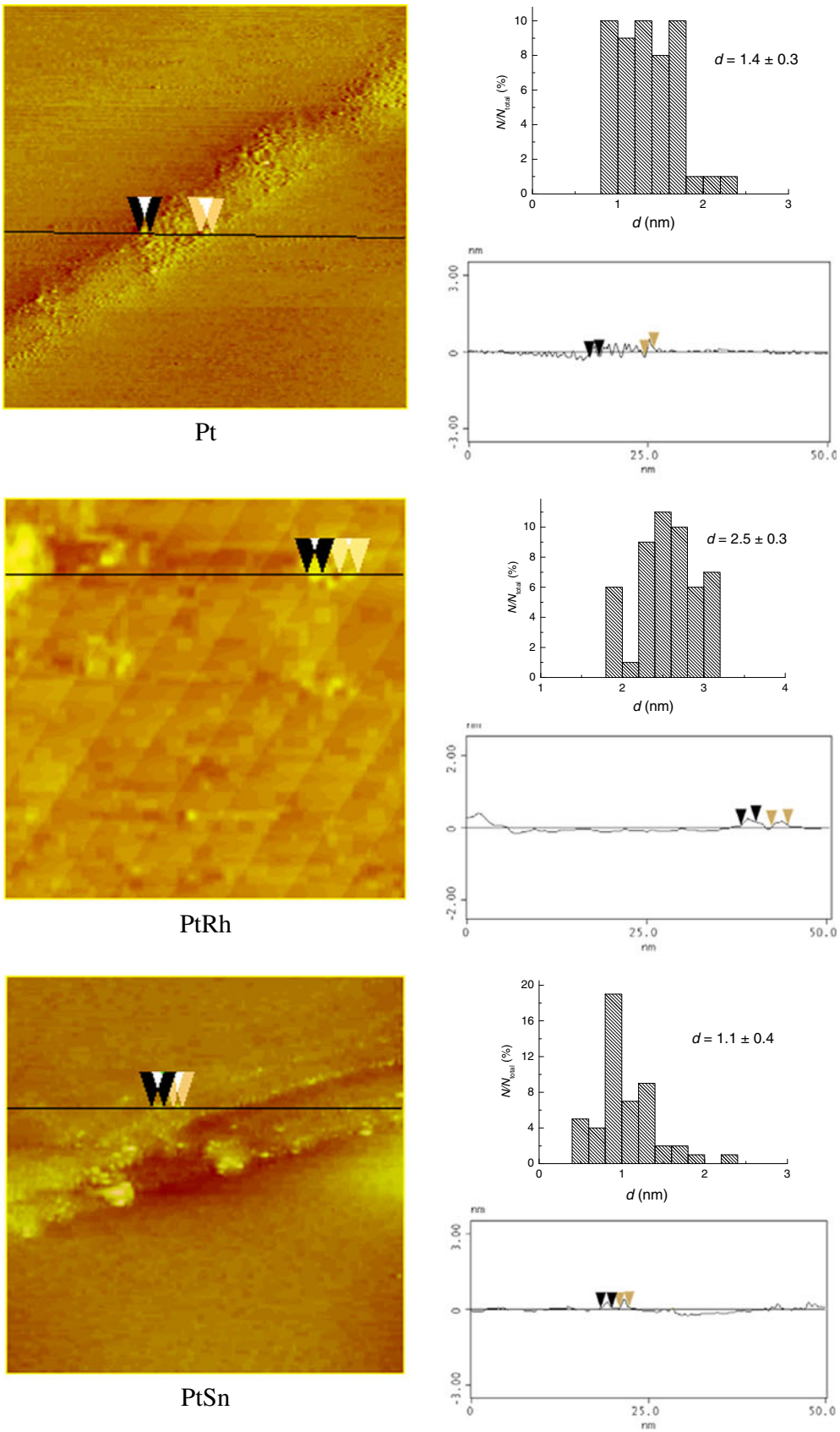

Fig. 1 STM images, cross-section analysis, and corresponding particle size distribution diagrams of Pt, PtRh, and PtSn unsupported catalysts (50×50×4 nm)

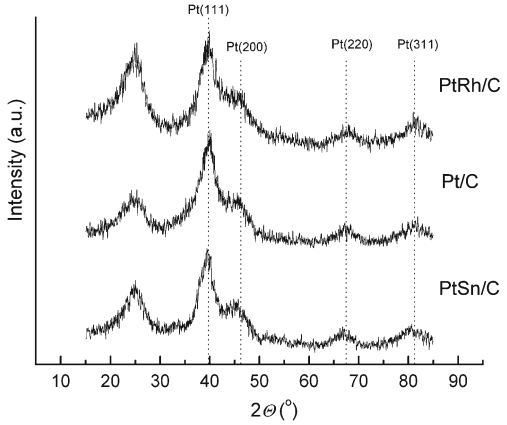

Fig. 2 XRD patterns of supported Pt/C, PtRh/C, and PtSn/C catalysts

shift of diffraction peaks of PtSn/C and PtRh/C catalysts with respect to Pt/C and the values of their lattice parameters should indicate the alloy formation between Pt and added metals but in low degree. The average crystallite size of each catalyst is calculated by Scherrer formula [36], and they are mutually similar, but for each catalyst larger than obtained by STM (Table 1). The reason for this difference is most probably because unsupported catalysts have been used for STM analysis, while XRD examinations have been performed with supported catalysts. Since the process of particle deposition onto the carbon support involves thermal treatment, it is possible that sintering of the particles occurred. Still, the agreement can be described as considerably good.

Typical TEM images of supported Pt-based catalysts (Pt/C, PtRh/C, and PtSn/C) and corresponding histograms of particle size distribution are displayed in Fig. 3. Observation of these images points out that catalyst particles are uniformly distributed on the carbon support. From the particle size histograms, it is obvious that the supported catalysts have similar particle size of ~3 nm which is in a very good agreement with the mean particles size evaluated from the XRD patterns. This confirms sintering of the metal particles obtained by microwave irradiation upon their deposition onto the carbon support and explains the difference with STM analysis of unsupported catalysts.

Although no peaks for metallic Rh or Sn or their oxides were detected by XRD, their presence should not be excluded, since they might be present in amorphous state or have a smaller particle size. Moreover, they should be present in a significant amount because EDX and TGA analyses of the catalysts have indicated practically no loss in the catalysts components. TGA revealed 20, 18, and 16 wt.% for Pt/C, PtSn/C, and PtRh/C catalyst, respectively. EDX compositions of bimetallic PtSn/C and PtRh/C catalysts (Table 1) slightly deviate from the nominal values.

Table 1 Pt/C, PtRh/C, and PtSn/C catalyst parameters obtained by STM, XRD, TEM, and EDX analyses

Catalyst	Pt/C	PtRh/C	PtSn/C
STM[a] Particle size (nm)	1.4±0.3	2.5±0.3	1.1±0.4
XRD Lattice parameter a (nm)	0.3944	0.3934	0.3963
XRD Particle size (nm)	2.5	2.6	2.6
TEM Particle size (nm)	2.7±0.8	3.1±0.7	2.4±0.7
Elemental composition Nominal (at.%)		50:50	50:50
Elemental composition EDX (at.%)		60.16:39.84	53.18:46.82

[a] STM analysis of unsupported catalyst particles

Electrochemical performances

Ethanol oxidation was studied at as-prepared Pt/C, PtRh/C, and PtSn/C catalysts. Therefore, the initial voltammograms, i.e., only 1 cycle for each of the catalysts have been recorded and presented in Fig. 4. Steady state cyclic voltammogram for Pt/C is given in the insert to illustrate similarity of this catalyst with polycrystalline platinum or other Pt catalysts supported on high area carbon [8, 13]. Cyclic voltammograms for Pt/C and PtSn/C are characterized by a defined region of hydrogen adsorption/desorption, separated by a double layer from the region of surface oxide formation. In the hydrogen adsorption/desorption region, the cyclic voltammogram for PtSn/C catalyst is similar to the voltammogram for Pt/C but with smaller currents due to a smaller amount of Pt sites on the surface. There is no clear boundary between hydrogen adsorption/desorption, double layer, and surface oxide regions in the cyclic voltammogram for the PtRh/C catalyst. The voltammogram reminds us of the one for such catalyst obtained by Lima et al. [9, 21], characterized by a large single peak in hydrogen adsorption/desorption region which the authors associated to adsorption/desorption of hydrogen on a PtRh intermetallic phase. Shift of reduction peak for PtRh/C to a more negative potential value in comparison to Pt/C should be an indication of more stable oxides of this catalyst [21].

The real surface area of the as-prepared catalysts was evaluated from CO stripping measurements (Fig. 5), assuming linear bonding of CO_{ads} [2, 9, 37]. This enabled calculation of particle size of Pt/C and PtRh/C catalysts supposing homogenous distribution of spherical-shaped particles from the equation [38]:

$$d = \frac{6000}{p \times S}$$

where S (square meter per gram) is specific surface area and ρ

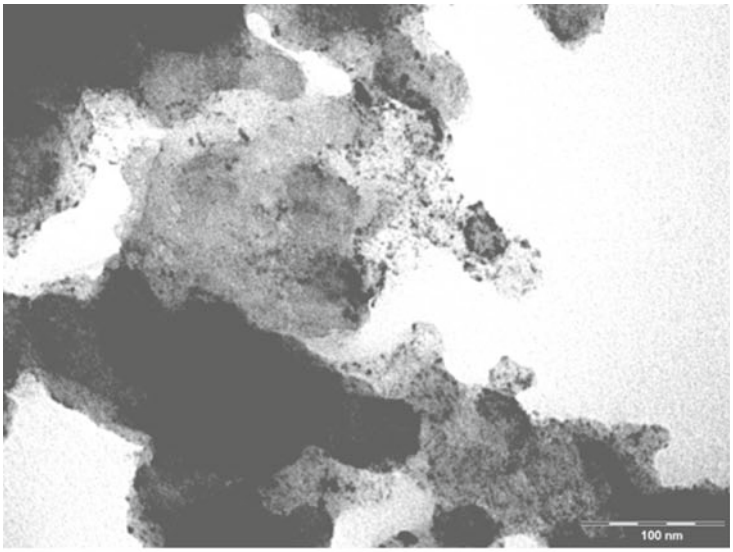

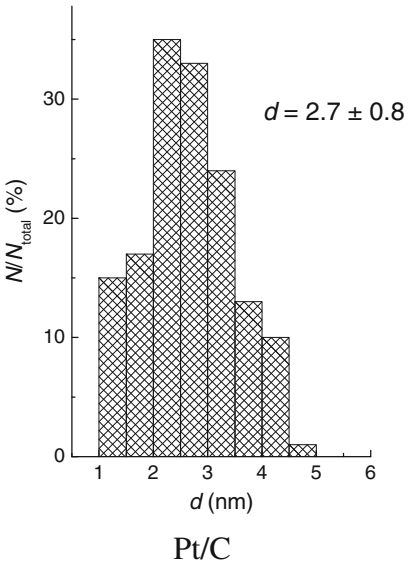

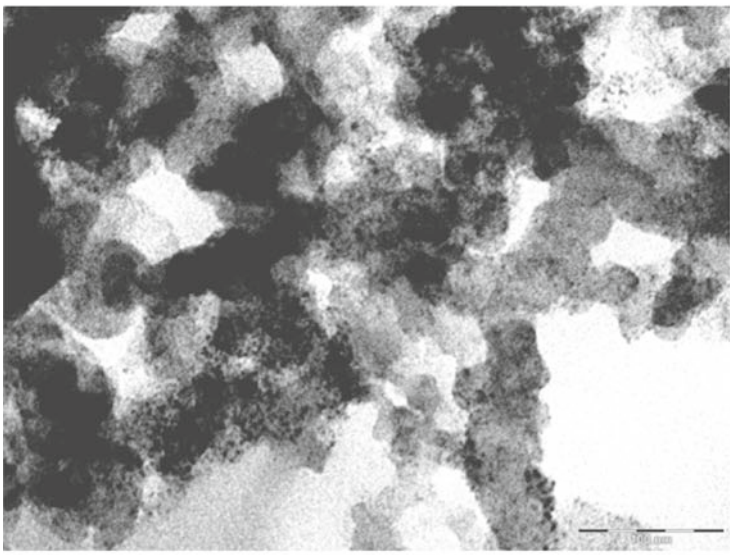

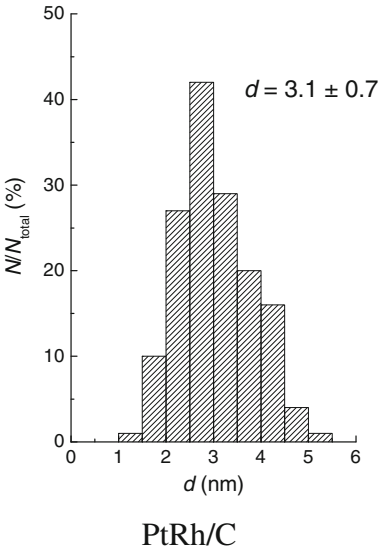

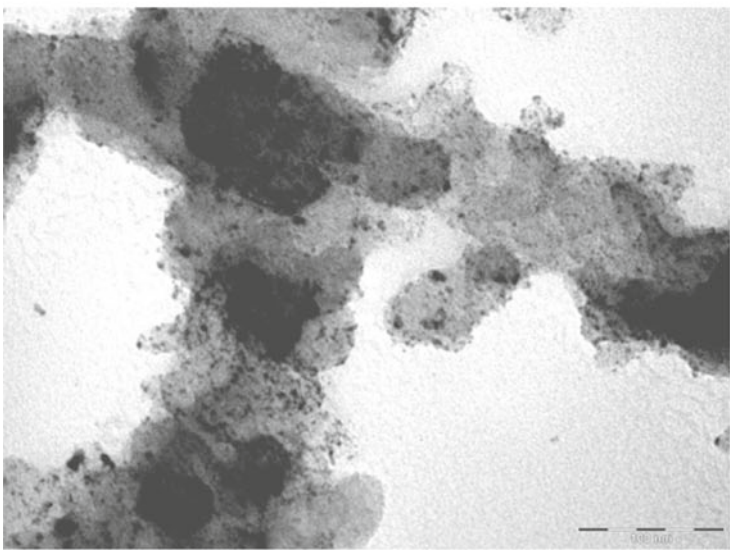

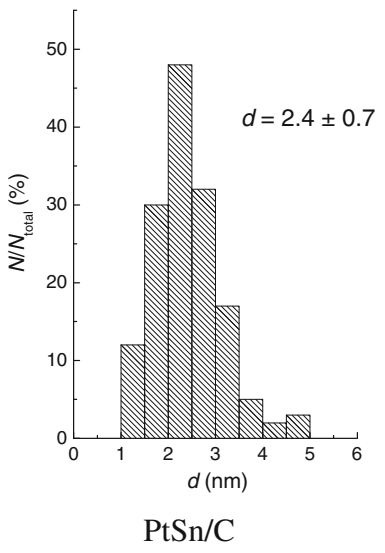

Fig. 3 TEM images and particle size distributions of supported Pt/C, PtRh/C, and PtSn/C catalysts

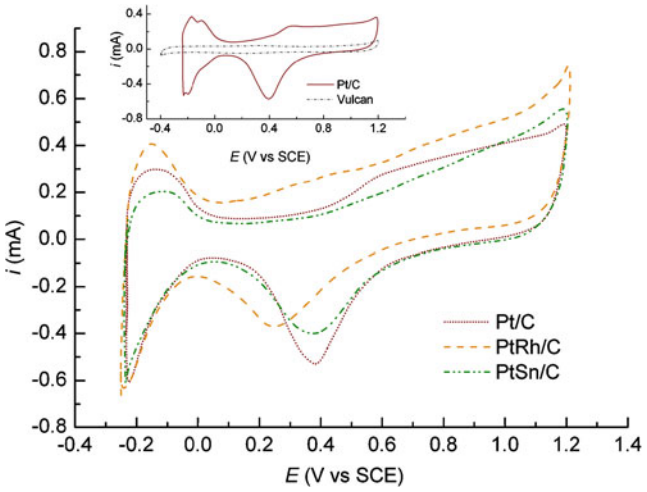

Fig. 4 Initial basic voltammograms of as-prepared Pt/C, PtRh/C, and PtSn/C catalysts in 0.1 M $HClO_4$, v=50 mV/s. *Insert* shows steady state CV of Pt/C catalyst and high-area carbon (Vulcan XC-72)

is the density of platinum or alloy. The density of alloy was calculated according to Chen et al. [39] from the equation:

$$\frac{1}{\rho_{PtM}} = \frac{\chi_{Pt}}{\rho_{Pt}} + \frac{\chi_{M}}{\rho_{M}}$$

where χ is the mass fraction of the metal in alloy.

Since CO does not adsorb at Sn [40], the real surface area for the PtSn/C catalyst refers only to Pt, and therefore, particle size for this catalyst cannot be evaluated. On the contrary, as CO adsorbs at Rh, the calculated real surface area of the PtRh/C catalyst then correlates to whole catalyst surface and enables particle size calculation. The data are presented in Table 2. The values obtained for the real surface area of the catalysts confirm that the surface composition corresponds to the bulk composition. So, for PtSn/C catalyst, the real surface area, which refers only to Pt, is 52 % of the real surface area of the Pt/C catalyst that coincides well with EDX result on the bulk composition of the PtSn/C catalyst. On the other hand, the values obtained for the particle size, being slightly higher than those obtained by

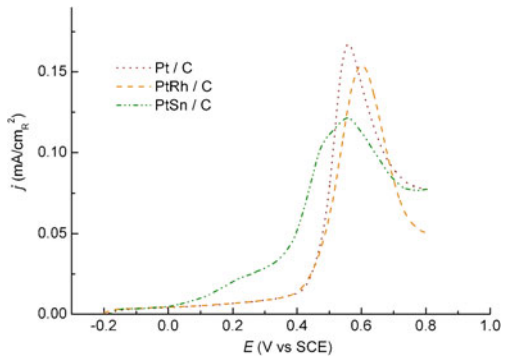

Fig. 5 CO_{ads} stripping curves for as-prepared Pt/C, PtRh/C, and PtSn/C catalysts in 0.1 M $HClO_4$, v=50 mV/s

Table 2 Particle size, real and specific surface areas of Pt/C, PtRh/C, and PtSn/C catalysts calculated from CO_{ads} stripping and TEM analyses

Catalyst	Pt/C	PtRh/C	PtSn/C
Real surface area (cm^2)	3.43	3.74	1.79
Mean particle size (nm)	3.3	3.4	n/a
Specific surface area (m^2/g)	85.8	93.5	81.4[a]
Specific surface area (TEM)[b] (m^2/g)	88.3	91.7	155.6

[a] Calculated only on Pt content

[b] S was calculated taking into account particle size and their fractions, i.e., size distribution

TEM, confirm agglomeration and sintering of the initial particles during deposition onto the carbon support. Also, a good agreement between values for the specific surface areas for Pt/C and PtRh/C, calculated using particle size obtained from TEM analysis and from the values for real surface area obtained by CO stripping, points out mainly monodispersion of the catalyst particles over the substrate. The large difference between these values for PtSn/C catalyst, is because the real surface area from CO stripping, refers only to Pt.

Oxidation of adsorbed CO monolayer enables not only the estimation of catalyst active surface area but also reveals the catalyst tolerance to CO. Observing the curves presented in Fig. 5, it can be noticed that at Pt/C, oxidation of CO commences somewhat before 0.4 V versus SCE and proceeds through a single sharp peak with current maximum at 0.55 V. The onset potential for CO oxidation at PtSn/C is shifted to lower values for more than 0.3 V, and the oxidation curve is significantly broadened as well as split into two peaks (shoulders). The latter one is centered at the potential value very close to the value of Pt/C, while the former is shifted for about 100 mV more negative and corresponds to CO oxidation peaks at Pt-Sn catalysts [12, 15]. Negative shift of the onset potential of CO oxidation at PtSn/C catalyst is attributed to the presence of oxygen-containing species at Sn at lower potentials in comparison to Pt as well as to the electronic effect of Sn on Pt [12, 15]. Two signals in the potential peak during oxidation of CO can be explained by low alloying degree of this catalyst and thus, part of nonalloyed Pt. Contrary to the case of PtSn/C, CO oxidation at PtRh/C commences at practically the same potential as at Pt/C. Since CO adsorption energy for Pt-CO is 125 kJ/mol and for Rh-CO is 134 kJ/mol [21], the addition of Rh to Pt in the PtRh catalyst might increase CO bond energy at PtRh, and although OH adsorbs at Rh at lower potentials in comparison to Pt, the oxidation of CO at PtRh is retarded.

The activity of the as-prepared Pt/C, PtRh/C, and PtSn/C catalysts for ethanol oxidation was evaluated from potentiodynamic and chronoamperometric measurements in 0.1 M

$HClO_4$+0.5 M C_2H_5OH solution. Potentiodynamic measurements were carried out in the potential range of technical interest, i.e., up to 0.3 V. This is also the range where no leaching of the second metal (Sn or Rh) can occur [5]. One anodic sweep at each catalyst was recorded in the extended potential region up to 0.8 V as well, in order to follow completeness of ethanol oxidation. The first anodic sweep recorded at each catalyst in low potential region is presented in Fig. 6. While PtSn/C exhibits significant activity related to Pt/C, there is almost no difference in electrocatalytic activity between PtRh/C and Pt/C catalysts. Ethanol oxidation commences at −0.15 V at as-prepared PtSn/C and proceeds with approximately three times higher currents in comparison to Pt/C. At higher potentials in the extended potential region (Fig. 7), PtSn/C remains more active than Pt/C, whereas PtRh/C losses its activity and becomes inferior in comparison to Pt/C. It should be mentioned here that Pt/C alone with onset potential for ethanol oxidation as well as the potential of anodic peak located at values lower for more than 0.1 V exhibits better performance compared to Pt/C catalysts described in literature [11, 32, 41, 42]. Analysis of the voltammetric curves in Figs. 6 and 7 point out that the

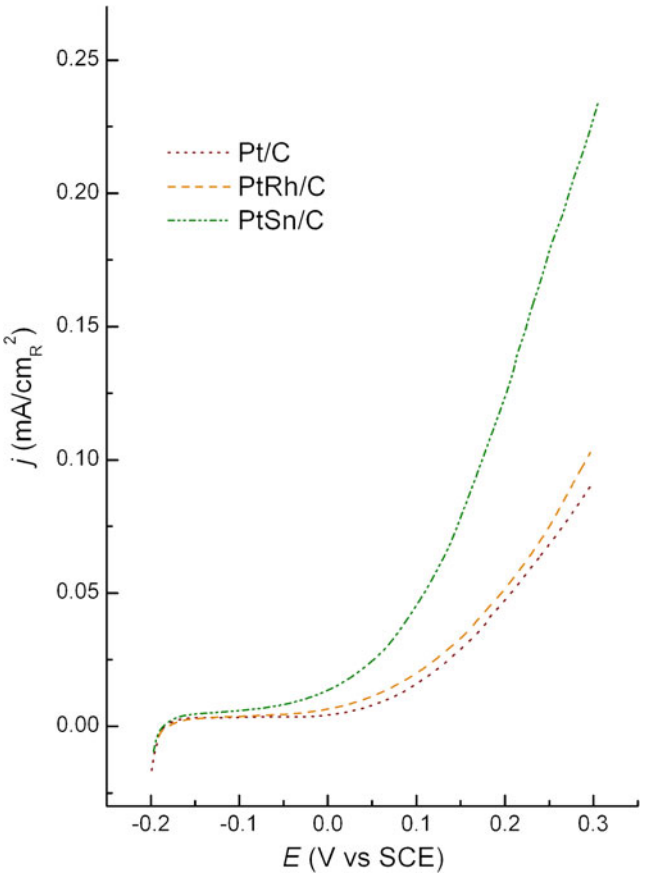

Fig. 6 Potentiodynamic curves in low potential region for the oxidation of 0.5 M C_2H_5OH at as-prepared Pt/C, PtRh/C, and PtSn/C catalysts in 0.1 M $HClO_4$, v=20 mV/s

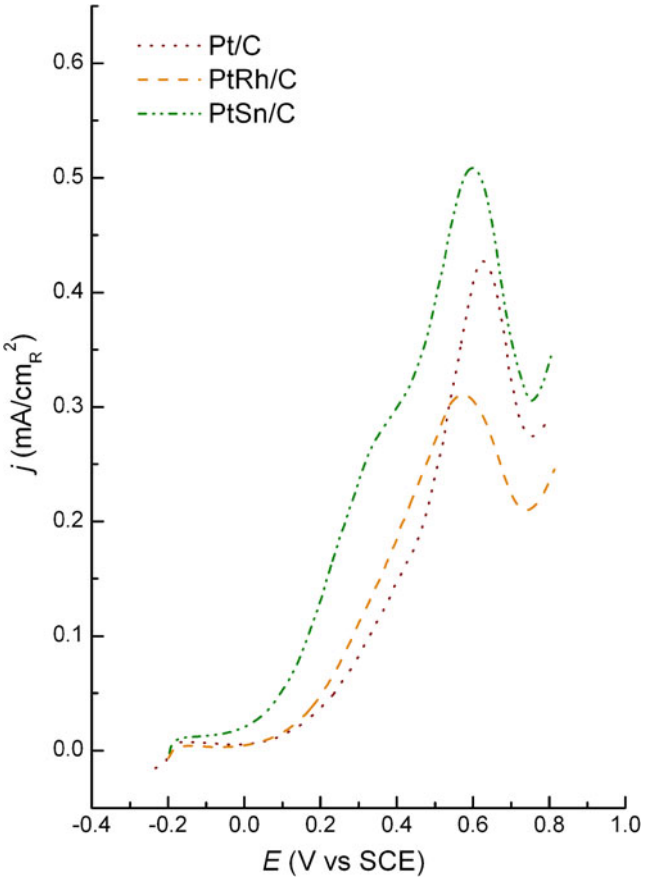

Fig. 7 Potentiodynamic curves for the oxidation of 0.5 M C_2H_5OH at as-prepared Pt/C, PtRh/C, and PtSn/C catalysts in 0.1 M $HClO_4$, v= 20 mV/s

addition of Sn in PtSn/C catalyst leads to a significant increase in activity in comparison to Pt/C specially at potentials of technical interest (lower than 0.3 V). The catalyst retains higher activity even in the extended potential region, but the current density increases less with the increase in potential. The initial potential for ethanol oxidation at as-prepared PtSn/C surface and the potential of anodic peak at 0.6 V are remarkably shifted to lower values in comparison to other PtSn catalysts with similar composition [5, 6, 8, 11, 32, 42, 43].

As already mentioned, the presence of Sn can promote ethanol oxidation by an electronic effect and/or by facilitating a bifunctional mechanism. Activation of interfacial water molecules leading to formation of OH species required for the oxidation of adsorbates generated by dehydrogenation of ethanol at adjusted Pt sites proceeds in Sn at lower potentials in comparison to Pt. In this way, by oxidation of $C_{1,ad}$ fragments (mostly CO_{ad}), formed by splitting of C–C bond, to CO_2 and $C_{2,ad}$ species with the intact C–C bond, i.e., acetaldehyde to acetic acid, a beneficial effect of Sn is in refreshing active Pt surface and supplying enough Pt active sites for adsorption and dissociation of ethanol [11, 32, 42].

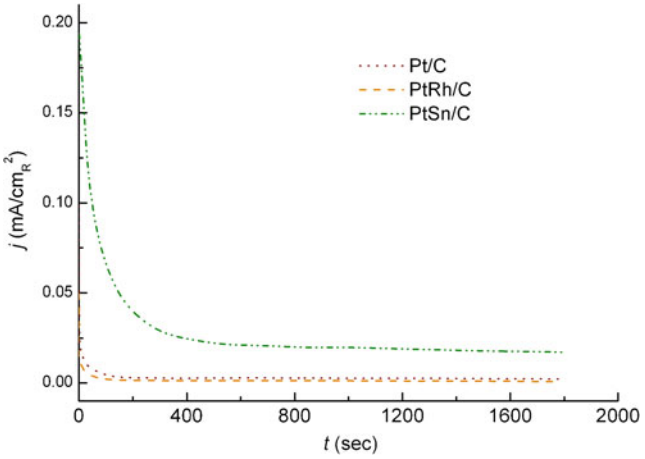

Fig. 8 Chronoamperometric curves for the oxidation of 0.5 M C_2H_5OH at as-prepared Pt/C, PtRh/C, and PtSn/C catalysts in 0.1 M $HClO_4$ at 0.2 V versus SCE

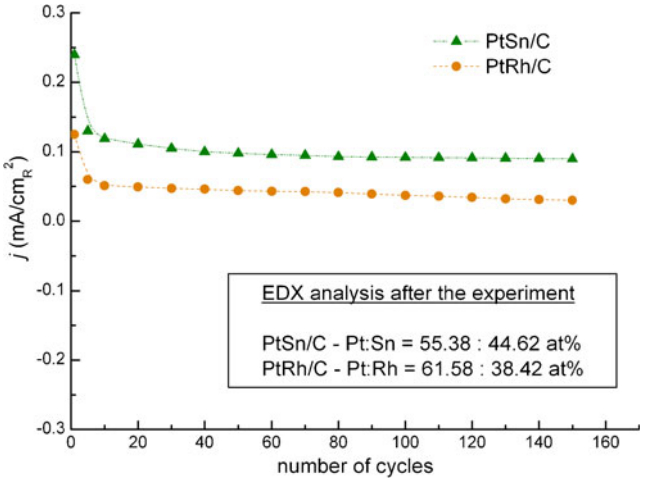

Fig. 10 Long-term stability of PtSn/C and PtRh/C catalysts in 0.1 M $HClO_4$+0.5 M C_2H_5OH versus number of scans, v=20 mV/s (current values are at 0.3 V)

Further, addition of Sn to Pt results in expansion of lattice parameter and elongation of bonding structure that changes geometric environment. The extended lattice parameter may enable C–C bond cleavage and thus, improve the catalytic activity [42]. Regarding the electronic effect, since Sn has four valence electrons available for modification of unfilled d band states of Pt atoms, this charge transfer from Sn atoms to neighboring Pt atoms may induce a weaker bond between adsorbates and Pt atoms. In the case of adsorbates with carbon atom, the poisoning of Pt should be reduced and adsorption of ethanol could also be diminished [42]. However, this charge transfer leads to easier formation of Sn oxide species, and these oxygen-containing species can facilitate electrooxidation of adsorbates on Pt sites at lower potentials.

XRD analysis of our PtSn/C catalyst reveals that the addition of Sn induced only slight extension of Pt–Pt distances resulting in rather low alloying degree. Since TG and EDX analyses indicated negligible loss of catalyst components, we could reasonably assume that significant quantity of nonalloyed Sn is present in the catalyst and on its surface. XPS and XRD analyses of bimetallic PtSn catalysts prepared by microwave-assisted polyol method identify a significant amount of SnO_2 and rather low alloying degree [28, 31, 32]. Thus, it is very likely that Sn in our PtSn/C catalyst is present mainly as SnO_2. The increased activity of our PtSn/C in comparison to Pt/C catalyst, therefore, is most probably enabled by a balanced ratio of Pt ensembles for ethanol dehydrogenation and C–C bond splitting and tin oxide for OH formation, i.e., by bifunctional mechanism although the electronic effect of alloyed Sn could play some role as well. In addition, high activity of as-prepared PtSn/C, and also Pt/C, catalyst could be supported by the presence of Pt adislands as well. These Pt adislands, i.e., highly undercoordinated Pt atoms on the catalyst surface are detected by STM on Pt single crystals and their remarkable activity in the oxidation of CO at lower potentials confirmed by FTIR [44]. Since polycrystalline Pt should have a number of such undercoordinated Pt atoms, they might as well contribute to the high activity of the catalysts.

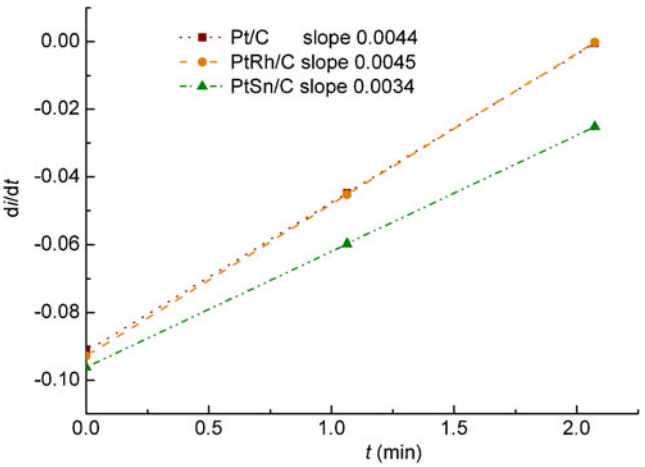

Fig. 9 di/dt versus time plots (from t=0 to t=120 s) for as-prepared Pt/C, PtRh/C, and PtSn/C catalysts

Contrary to PtSn/C, PtRh/C catalyst exhibits similar activity for ethanol oxidation as Pt/C at potentials of technical interest, i.e., up to 0.3 V (Fig. 6). At higher potentials, the faradeic currents at PtRh/C are lower in comparison to Pt/C (Fig. 7). Such behavior of the catalyst is in accordance with literature data [9, 20, 21] for PtRh catalysts of similar Pt to Rh molar ratio, with the exception for onset potential, since the oxidation of ethanol commences at our PtRh/C at lower values. According to Bergamaski et al. [20, 21] Rh is less efficient for dehydrogenation of ethanol than Pt, and the high-energy barrier for dehydrogenation can lower reaction rate at surfaces containing Rh. Another reason for a low

reaction rate at PtRh catalysts might be difficulty in electrooxidation of CO on Rh because of stronger O–Rh bonding in comparison to Pt–O that can result in higher activation energy for CO–O coupling and thus hinder CO oxidation [20]. In this sense, small particle size plays an important role, since small particles are more oxophylic. Still, DEMS and FTIR studies revealed improved CO_2 and decreased acetaldehyde yields at PtRh surfaces that should mean that the role of Rh in PtRh catalysts is more likely to increase C–C bond splitting and not provide oxygen more readily for CO electrooxidation [20].

To examine the poisoning tolerance of our Pt/C, PtRh/C, and PtSn/C catalysts during ethanol oxidation, chronoamperometric experiments have been performed, and the results are presented in Fig. 8. The PtSn/C catalyst exhibits higher initial current density at 0.2 V, while Pt/C and PtRh/C demonstrate similar behavior with lower currents, which is in accordance with potentiodynamic measurements (Fig. 6). In Pt/C and PtRh/C catalysts, contrary to PtSn/C, current decay rapidly and reaches low steady state values in a few minutes. Current decreases slowly at PtSn/C and stabilizes at the value which is significantly higher than for two other catalysts in the experimental time period. This proves that PtSn/C is considerably less poisoned than Pt/C or PtRh/C. Lower poisoning of PtSn/C is confirmed by di/dt as a function of t for short period of time (t from 0 to 2 min.) (Fig. 9). A smaller value of the slope means lower initial poisoning of the electrode surface [45]. Thus, it appears that the addition of Sn to Pt facilitates lower poisoning compared to Pt/C or PtRh/C, since the experimental slope is lower by factors 1.29 and 1.33, respectively.

In addition, long-term stability of PtSn/C and PtRh/C catalysts was tested for ethanol oxidation in 0.1 M $HClO_4$ during 150 cycles in the potential range of technical interest, i.e., between −0.2 V and 0.3 V. The results are presented in Fig. 10 as the current value at 0.3 V versus number of the cycle. For both catalysts after initial decrease during the first 5 cycles, decline in current values is significantly retarded and for PtSn/C at the end of the test is about 70 % lower in comparison to the fifth cycle, while for PtRh/C, it is about 50 %. This loss in catalyst activity may be due to the poisoning of the surface or to leaching of the added non-noble metal. To test leaching of Sn and Rh, the PtSn/C and PtRh/C electrodes were examined by EDX after the experiments and the results are shown in Fig. 10 as well. These analyses revealed minor leaching of both metals from bimetallic catalysts and confirmed their stability.

Conclusions

Ethanol oxidation reaction was studied at carbon-supported Pt/C, PtRh/C, and PtSn/C catalysts prepared by microwave-assisted polyol procedure. According to lattice constants obtained from XRD analysis, low alloyed PtSn and PtRh catalysts were obtained. STM examinations revealed that unsupported catalysts have rather uniform small particles of approximately 2 nm. This should be attributed to the advantages of microwave-assisted polyol process in EG solution. During deposition of catalyst particles onto the carbon substrate and thermal treatment, sintering and agglomeration occur, and supported catalysts as determined by TEM have somewhat larger particles of approximately 3 nm.

It is found that the activity of Pt-based bimetallic catalyst for ethanol oxidation greatly depends on secondary metal and the electrode potential. While addition of Sn to Pt leads to the significant enhancement of ethanol oxidation and lower poisoning of electrode surface, addition of Rh only modestly changes overall electrochemical reaction. The onset potential for ethanol oxidation at our PtSn/C catalyst is remarkably shifted to lower values in comparison to other PtSn catalysts with similar composition. The increased activity of PtSn/C catalyst is mainly due to a bifunctional mechanism, enabled most probably by nonalloyed Sn (SnO_2), although an electronic effect of low alloyed PtSn could play some role as well.

Acknowledgments This work was financially supported by the Ministry of Education and Science, Republic of Serbia, Contract No. 172060.

References

1. Antolini E (2007) J Power Sources 170:1–12
2. Wang Q, Sun GQ, Jiang LH, Xin Q, Sun SG, Jiang YX, Chen SP, Jusys Z, Behm RJ (2007) Phys Chem Chem Phys 9:2686–2696
3. Zhou W, Zhou Z, Song S, Li W, Sun G, Tsiakaras P, Xin Q (2003) App Catal B 46:273–285
4. Tsiakaras PE (2007) J Power Sorces 171:107–112
5. Kowal A, Gojković SLj, Lee K-S, Olszewski P, Sung Y-E (2009) Electrochem Commun 11:724–727
6. Colmati F, Antolini E, Gonzalez ER (2008) J Alloys Compd 456:264–270
7. Wang H, Jusys Z, Behm RJ (2006) J Power Sources 154:351–359
8. Li H, Sun G, Cao L, Jiang L, Xin Q (2007) Electrochim Acta 52:6622–6629
9. Lima FHB, Profeti D, Lizcano-Valbuena WH, Ticianelli EA, Gonzalez ER (2008) J Electroanal Chem 617:121–129
10. Sen Gupta S, Datta J (2006) J Electroanal Chem 594:65–72
11. Simões FC, Dos Anjos DM, Vigier F, Léger J-M, Hahn F, Coutanaceau C, Gonzalez ER, Tremiliosi-Filho G, De Andrade AR, Olivi P, Kokoh KB (2007) J Power Sources 167:1–10
12. Vigier F, Coutanceau C, Hahn F, Belgsir EM, Lamy C (2004) J Electroanal Chem 563:81–89
13. Colmenares L, Wang H, Jusys Z, Jiang L, Yan S, Sun GQ, Behm RJ (2006) Electrochim Acta 52:221–233
14. Zhu M, Sun G, Xin Q (2009) Electrochim Acta 54:1511–1518
15. Godoi DRM, Perez J, Villullas HM (2010) J Power Sources 195:3394–3401
16. Liu P, Logadottir A, Norskov JK (2003) Electrochim Acta 48:3731–3742

17. Jiang L, Sun G, Sun S, Liu J, Tang S, Li H, Zhou B, Xin Q (2005) Electrochim Acta 50:5384–5389
18. Delime F, Léger J-M, Lamy C (1999) J Appl Electrochem 29:1249–1254
19. Jiang L, Colmenares L, Jusys Z, Sun GQ, Behm RJ (2007) Electrochim Acta 53:377–389
20. De Souza JPI, Queiroz SL, Bergamaski K, Gonzalez ER, Nart FC (2002) J Phys Chem B 106:9825–9830
21. Bergamaski K, Gonzalez ER, Nart FC (2008) Electrochim Acta 53:4396–4406
22. Wang Y, Zhang J, Wang X, Ren J, Zuo B, Tang Y (2005) Topics in Catalysis 35:35–41
23. Feldmann C, Metzmacher C (2001) J Mater Chem 11:2603–2606
24. Yu W, Tu W, Liu H (1999) Langmuir 15:6–9
25. Knupp SL, Li W, Paschos O, Murray TM, Snyder J, Haldar P (2008) Carbon 46:1276–1284
26. Tu W, Liu H (2000) Chem Mater 12:564–567
27. Tu W, Liu H (2000) J Mater Chem 10:2207–2211
28. Liu Z, Guo B, Hong L, Lim TH (2006) Electrochem Commun 8:83–90
29. Rao KJ, Vaidhyanathan B, Ganguli M, Ramakrishnan PA (1999) Chem Mater 11:882–895
30. Chen WX, Lee JY, Liu Z (2002) Chem Commun 2588–2589
31. Liu Z, Hong L, Tay SW (2007) Mater Chem Phys 105:222–228
32. Wang Y, Song S, Andreadis G, Liu H, Tsiakaras P (2011) J Power Sources 196:4980–4986
33. Kraus W, Nolze G, (2000) PowderCell for Windows, V.2.4, Federal Institute for Materials Research and Testing Berlin, Germany
34. Von Weast RC (1966) Handbook of chemistry and physics, 47th edn. The chemical Rubber Co., Cleveland, OH
35. Fievet F, Lagier JP, Blin B, Beaudoin B, Figlarz M (1989) Solid State Ionics 32–33:198–205
36. Klug HP, Alexander LE (1974) X-ray diffraction procedures 2nd ed. Wiley, New York
37. García G, Silva-Chong JA, Guillén-Villafuerte O, Rodríguez JL, González ER, Pastor E (2006) Catal Today 116:415–421
38. Gloaguen F, Léger JM, Lamy C, Marmann A, Stimming U, Vogel R (1999) Electrochim Acta 44:1805–1816
39. Chen YA, Bandeira IN, Rowe OM, Min G (1994) J Mater Sci Letters 13:1051–1053
40. Shubina TE, Koper MTM (2002) Electrochim Acta 47:3621–3628
41. Lamy C, Rousseau S, Belgsir EM, Coutanceau C, Léger J-M (2004) Electrochim Acta 49:3901–3908
42. Kim JH, Choi SM, Nam SH, Seo MH, Choi SH, Kim WB (2008) Appl Catal B 82:89–102
43. Jiang L, Sun G, Zhou Z, Zhou W, Xin Q (2004) Catal Today 93–95:665–670
44. Strmcnik DS, Tripkovic DV, Van der Vliet D, Chang KC, Komanicky V, You H, Karapetrov G, Greeley JP, Stamenkovic VR, Markovic NM (2008) J Am Chem Soc 130:15332–15339
45. Delime F, Léger JM, Lamy C (1998) J Appl Electrochem 28:27–35